CAPELLA SPACE X-BAND SYNTHETIC APERTURE RADAR (SAR) DATA FOR ENVIRONMENTAL AND HUMANITARIAN USE CASES IN EARTH OBSERVATION

Katina Mattingly (1), Shaunak De (1)

(1) Capella Space, 438 Shotwell St, San Francisco CA 94110, +1-415-481-4727, katina.mattingly@capellaspace.com

Abstract: Capella Space is a Synthetic Aperture Radar (SAR) Small-Sat company that designs, builds, and operates 100-kg class spacecraft to produce very-high resolution commercially available X-band SAR data. Since the start of commercial operations in January 2021 with its flagship spacecraft, Capella has launched multiple additional satellites, producing enormous amounts of earth observation data. It is our goal in this proceeding at the 4S Symposium to introduce the small-sat community to Capella Space's new mission capability, share details of the spacecraft, and introduce the unique capabilities of Capella SAR data for earth observation. Topics of study are focused on environment and humanitarian applications including:

1. **Infrastructure mapping**: The global population is rapidly urbanizing. Semantic segmentation of SAR backscatter can classify ground cover types and identify the extent of urban areas at any given time.
2. **Rice crop dynamics**: Rice cropping presents altering backscatter returns in different stages of the phenology which can be used to understand crop dynamics and make yield predictions, critical parameters for a staple crop in many countries.
3. **Glaciers**: SAR data can help derive flow velocity, surface elevation change, mass balance, calving front location, delineate glacial zones (facies) and other critical parameters.

These are just a small sample of the earth science and humanitarian missions that SAR can address. Cloud penetration, 24/7 imaging, and large area cover of remote locations make SAR a cost effective and powerful tool for understanding glaciers. Figure 1 is Capella SAR imagery over Ruth Glacier, Helheim Glacier, and a rice cropping area in Bangladesh, which are used in this paper:

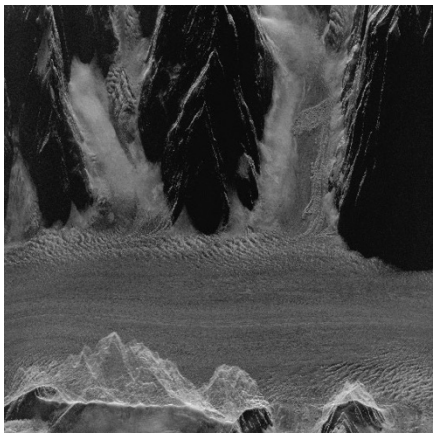

(a)

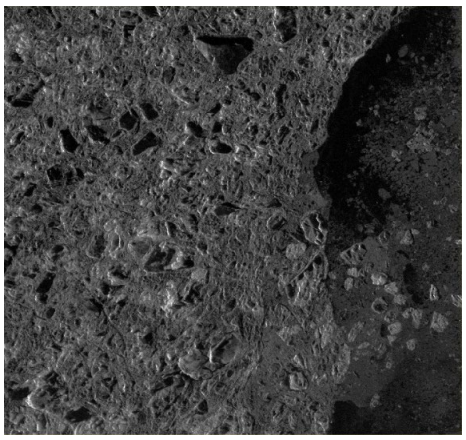

(b)

Label	Mean dB
Harvested (blue)	-12.57
Forest (red)	-8.83
Growing Rice (yellow)	-5.16
Inundated Paddy (cyan)	-19.82

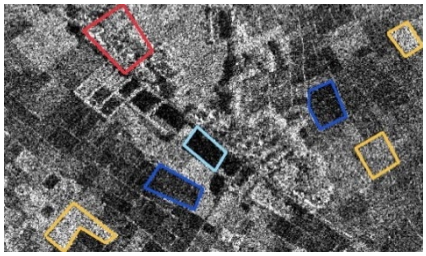

(c)

Figure 1 (a) Capella SAR image of Ruth Glacier in Denali National Park, Alaska captured on 2021-12-27, spotlight image mode, HH polarization. The main glacier body can be seen horizontally across the image with flow features in the center and crevasses along the edge. (b) Capella SAR image of Helheim Glacier in Greenland captured on 2021-12-14, past the calving front as compacted snow and ice meet open water, spotlight imaging mode, HH pol. (c) Mean backscatter return in dB of rice crop stages with corresponding areas in a Capella SAR stripmap image over Bangladesh, HH pol.

About Capella Space:

Capella Space is a commercial SAR provider owned and operated in the US that designs, builds, operates and distributes data from its constellation of X-band SAR satellites. With multiple operational spacecraft, Capella offers unique earth remote sensing capabilities with high frequency revisit, very high-resolution imagery, and a modern system for tasking, requesting, and accessing data. The current spacecraft constellation operates at 9.65 GHz center frequency, up to 500 MHz bandwidth and 600 W radar transmit power. This produces very high quality and high-resolution SAR data. The spacecraft are single-polarized and nominally collect HH (transmit horizontal, receive horizontal), but can also collect VV (transmit vertical, receive vertical) based on the user's applications. Capella performs three main imaging modes of spotlight, sliding spotlight and stripmap, which trade resolution against area ground cover. For example, spotlight mode produces a 50 cm by 50 cm ground plane resolution product with a 5 km by 5 km footprint, while stripmap mode produces a 1.2 cm by 1.2 cm ground plane resolution product with a 5 km by 20 km footprint. Each imaging mode has a corresponding standard product called Spot (spotlight mode), Site (sliding spotlight) and Strip (stripmap)[1]. Users of the Capella Space system have the ability to select imaging parameters and mode to suite their specific use cases. See Figure 2 for sample imagery

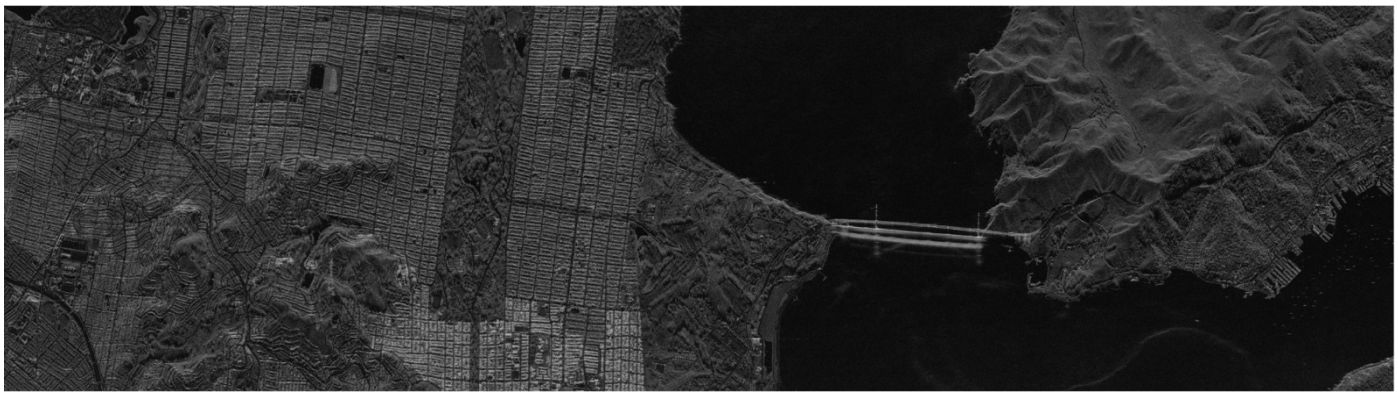

Parameter	Specification
Frequency	9.65 GHz (X-Band)
Output Power	600 W peak at 20% duty cycle
Imaging Bandwidth	500 MHz
Polarizations	Single Pol HH or Single Pol VV
Slant-plane Range Resolution	0.3 m
Acquisition Direction	Left and right sides
Imaging Modes	Spotlight, Sliding Spotlight, Stripmap
On-Board Storage	3TB
On-Board Processor	NVIDIA GPU
Payload Duty Cycle	Up to 10% (CONOPS dependent)
Antenna Aperture	8 m^2 class

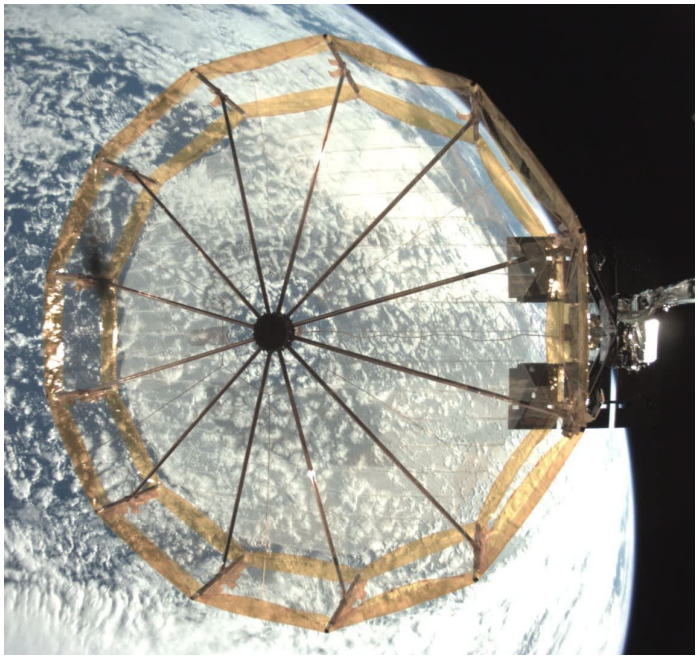

Figure 2 Top: A Capella Space SAR stripmap image of San Francisco including the Golden Gate Bridge center right, the Marin headlands to the right, Golden Gate Park center left, and Twin Peaks to the left. Resolution is 1.2 m square on the ground plane. Bottom right: Image taken from onboard cameras of Capella's payload reflector antenna with the clouded earth present in background. Bottom left: design specs of the Capella Space smallsat X-band SAR satellite [1].

over San Francisco, an actual image taken of the Capella Space reflector from space, and a table describing some spacecraft performance parameters.

Capella space has complimented high quality SAR data with automated operations and an easy to use console platform for data searching, ordering and downloading. Communication and data downlink with the satellites are performed using a constellation of commercial ground-as-a-service partners, providing global and frequent ground contacts. This allows for near constant up-linking of schedules to optimize collections across the constellation and the rapid downlink of imagery data. The constellation also uses a persistent GEO communication link to enable low-volume time sensitive coms. All space operations of the fleet are done by in-house Capella developed software. Once SAR imagery is downlinked it is processed, quality checked and delivered to users automatically using a modern cloud-based infrastructure. Beyond commanding the spacecraft to perform a new collection (tasking), users also have the option to access existing SAR data from the Capella archive for historical or time-series data. To task spacecraft, search for data, download data and more, Capella has built a web-based console and a companion API. The Capella console is very easy to use with an intuitive map interface while the API allows for more fidelity in tasking parameters and can be integrated into automated workflows [*2*].

1. INFRASTRUCTURE MAPPING

The economic changes over the last two decades have incentivized populations the world over to rapidly urbanize. Migration of people from rural areas to urban population centers are primarily driven by the increased access to economic opportunities and social mobility in cities. Already over 50 percent of the human population is urban, with this expected to rise to 69% by 2050 [*3*]. The largest of these migrations are expected to happen in developing nations, which are already host to some of the fastest growing cities in the world.

In the past few decades, there has been a rapid rise in remotely sensed imagery acquired by space- or airborne sensors. This has enabled unprecedented ability to observe large areas with high temporal density, enabling large scale monitoring or dynamic earth processes like urbanization. This long-term monitoring ability has allowed us to characterize anthropocentric growth in remote areas, or in countries without strong government mapping and survey programs. VHR monitoring of these regions will help local governments plan for infrastructure and support. Semantic segmentation of SAR backscatter can classify ground cover types and identify extent of urban areas at any given time. In addition, Coherent Change Detection (CCD) is a technique common to SAR imaging that can help identify changes between collects [4, 5].

Spaceborne optical sensors can deliver global coverage with high spatial, temporal, and spectral resolution, but these passive sensors are limited because they cannot image during the night or in inclement weather. Additionally, for several regions, the urban housing stock is made up of low settlements constructed by earth, or earth-like materials which can be hard to discerner in optical imagery. The active properties of SAR imaging can be exploited to improve urban area mapping. Since SAR sensors are not dependent on external sources for illumination, and radar wavelengths have cloud penetrating capabilities, these sensors are able to operate without restriction of time and season. Since SAR is more dependent on the physical properties and geometry of the target rather than the color, it can be more useful for unsupervised global urban mapping applications. A swath of Capella's VHR imagery in X-Band SAR collected over Gwagwalada, Nigeria is presented in Figure 3 and Figure 5. Even with the backscatter image alone, it is possible to see the brighter urban areas separated from its surroundings. This is one of the fastest growing urban centers on earth [*7*] and monitoring it's expansion is critical for infrastructure planning to support the influx of people.

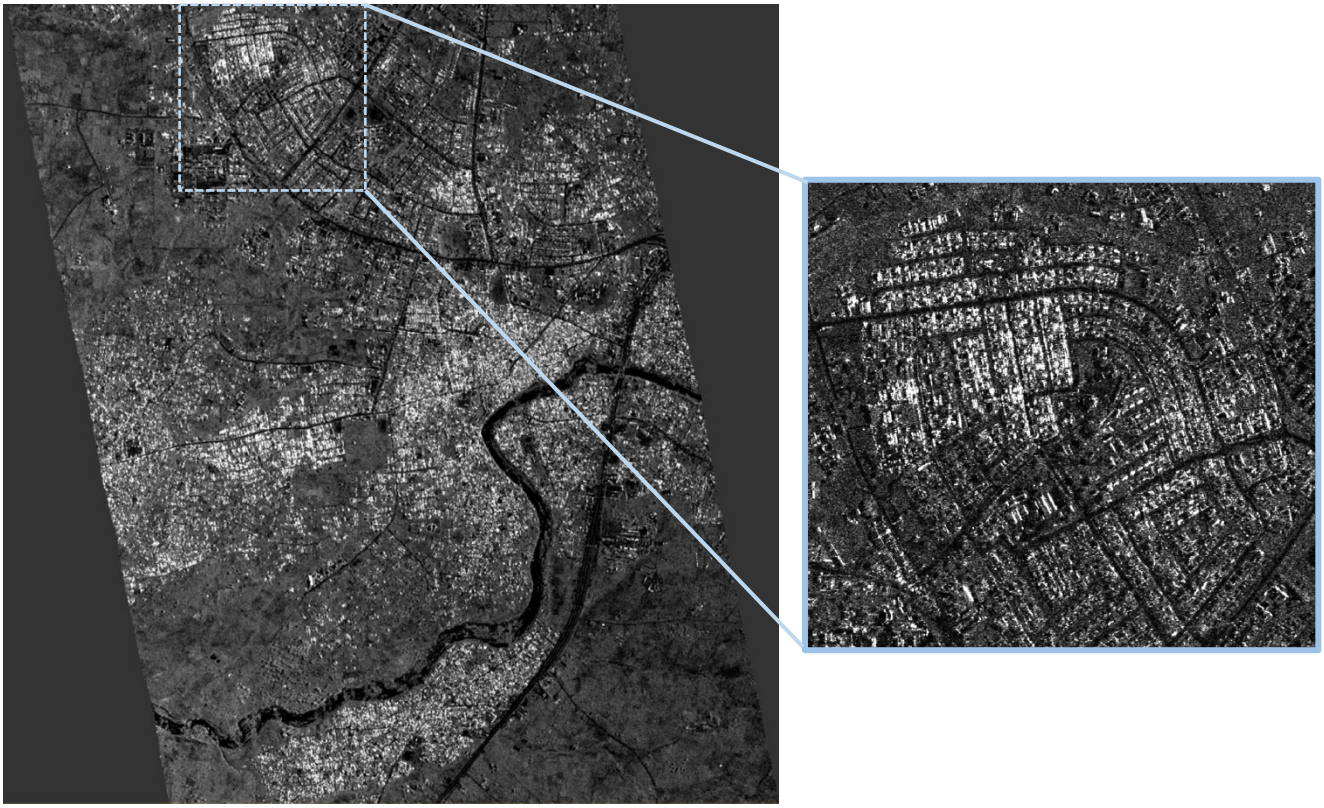

Figure 3: Capella VHR Stripmap imagery acquired over Gwagwalada, Nigeria showing the rapidly growing urban agglomeration. In the zoomed in figure on the right, it is easy to distinguish roadways and building patterns.

Because a high concentration of human population lives in urban areas, it becomes important to monitor the growth and expansion of these areas – especially in the case of time sensitive events like natural calamities like floods, earthquakes and tsunamis. It is important to derive information as rapidly as possible to help with disaster-management applications. An accurate urban map can be cross-referenced against post-event data to help save lives and provide relief and support. Several high-growth urban areas are in tropical regions – which remain un-imageable by optical sensors for several months in the year due to the onset of the monsoon season. During this time, these areas are at a higher risk of flooding. SAR becomes one of the only few ways of performing routine or on-demand monitoring of these areas.

Accurate urban maps are crucial for resource planning, transport network capacity modeling, and vulnerability mapping on a local scale for planning activities. At a higher level, aggregated urban area metrics like population density, built landcover area etc. are very useful for global climatic modelling. In this era of unprecedented anthropogenic climate change, measurement of built-up urban area and its year-over-year growth can be an important input variable in complex climate relationship models [*8*].

The workflow to generate urban area maps from VHR SAR data is presented in Figure 6 and a demonstration of the data layers is shown in Figure 7. The Coefficient of Variation (COV) is computed on the input SAR image on a N × N window using the mean and standard deviation. The value of N is determined by the desired minimum mapping unit, and by the spatial resolution of the underlying SAR data. For Capella VHR Stripmap, a value of N=11 was found to be an ideal balance of accuracy of output and mapping resolution. The COV is computed by,

$$I_{urban} = \sum_{1}^{N^2} \mu_{N\times N} / \sigma_{N\times N}$$

Here, I_{urban} is the urban area metric, which needs to be thresholded to form an urban area map. This is done by using the Otsu global thresholding algorithm, the output of which is geocoded to form the final urban area map.

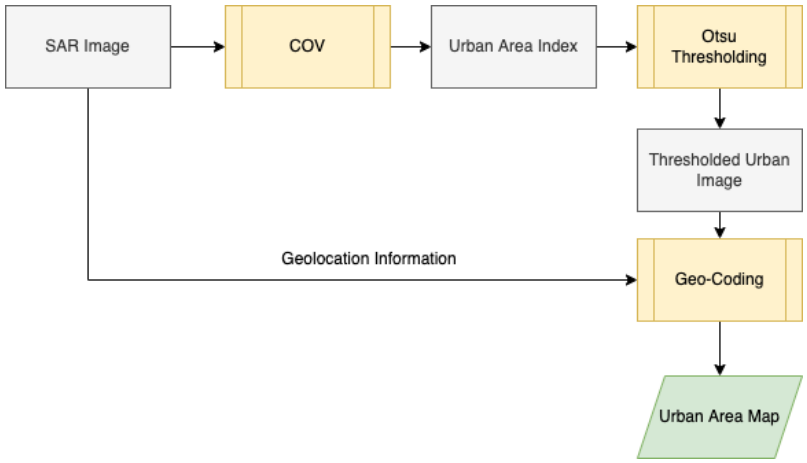

Figure 4 Urban Area Map generation workflow from SAR VHR imagery.

The Otsu thresholding algorithm is commonly used in computer vision applications to threshold images that have a bimodal histogram, but discovering the valley point between the two modes. There are several implementations of Otsu available, we use the one contained in Scipy python library. The difference in scattering statistics from highly coherent urban targets, and bragg type scattering from the surrounding areas is what is exploited here to enable the separability.

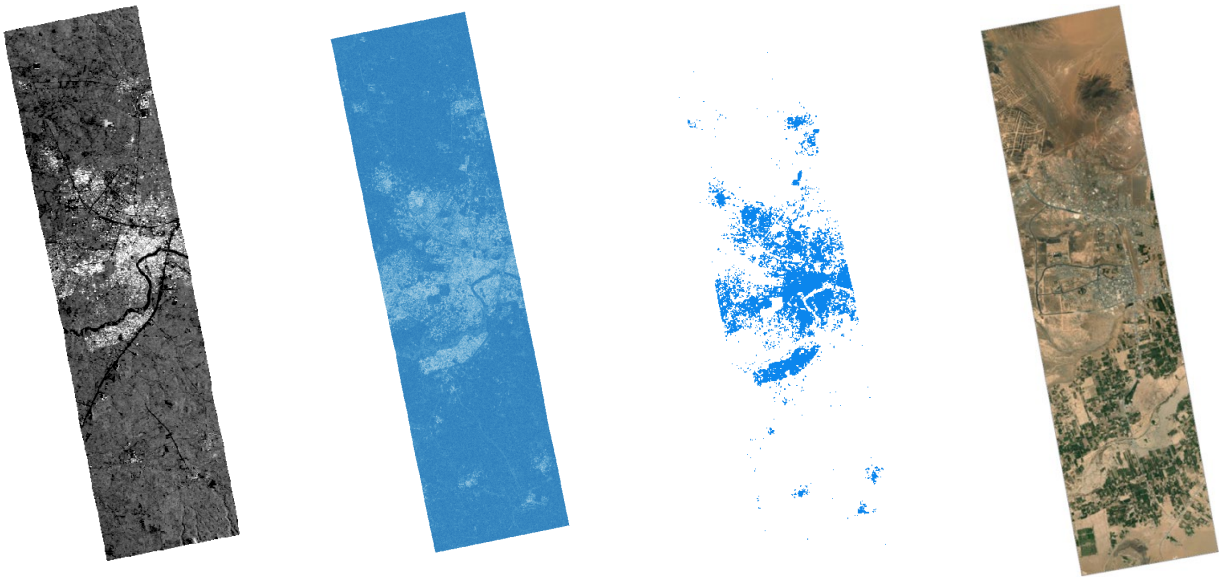

(a) SAR Backscatter *(b) COV* *(c) Otsu* *(d) Base-map*

Figure 5 Visualization of the data-layers as they move through the data pipeline. The (a) SAR Backscatter from one scene over Gwagwalada, Nigera is shown. The (b) COV metric is computed from this and the resultant is plotted. This is then passed through an automatic segmentation algorithm, i.e. (c) Otsu Global threshold and the (d) optical basemap from Microsoft Bing is shown for comparison

SAR is a side-looking imaging modality. This is primarily because imaging in a nadir looking manner would cause an ambiguity in resolving the direction of range echoes. Due to this, challenges exist in urban area mapping since changes in the angle of imaging can cause shifts in positioning of the urban

target in VHR imagery, depending on the height of the target. Geometric artifacts like layover, foreshadow and shadow effects are common sources of error in urban mapping with VHR SAR. Uncertainty contributions from these sources can be reduced by averaging or stacking urban area maps from several scenes. Care must be taken to select scenes that don't have a mix of look-directions (select either Left or Right) and orbits (Descending or Ascending).

Figure 8 shows urban area maps generated from several Capella VHR collects computed over Marib, Yemen and Gwagwalada, Nigeria. A stack of 3 images is acquired over Gwagwalada, Nigeria between a period of 2021-11-12 to 2022-02-09 and the mean urbanized area is computed to be 11.72 ± 2.33 km. sq over the entire scene footprint. Similarly, 5 images are computed over Marib, Yemen between 2021-11-18 and 2022-03-02 and the mean urbanized area is computed as 12.94 ± 3.26 km. sq over the entire scene footprint.

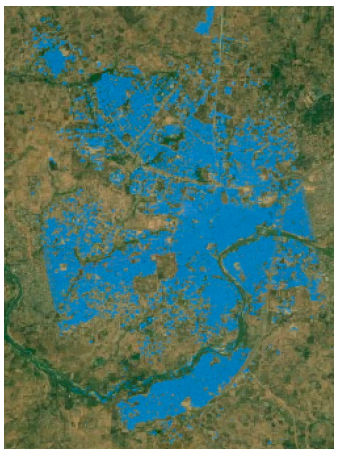

Composite Urban Area Map, apr. 11 km sq – Gwagwalada Nigeria

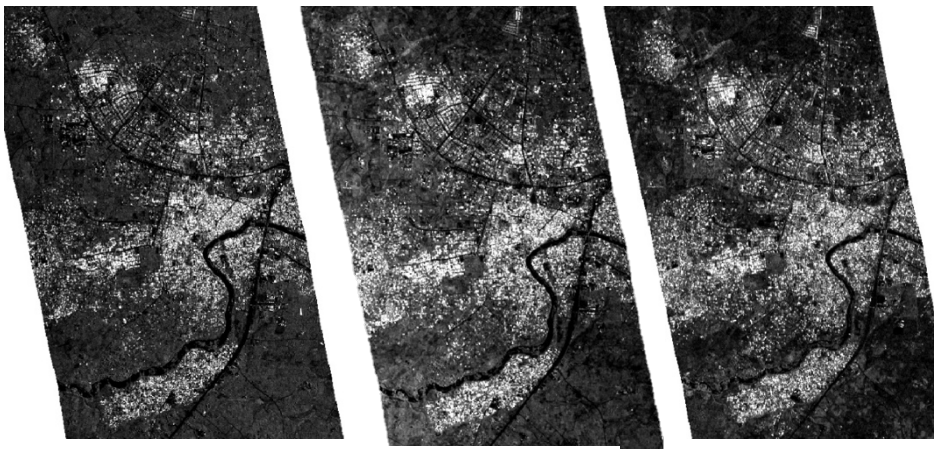

2021-11-12 2021- 12-15 2022-02-09

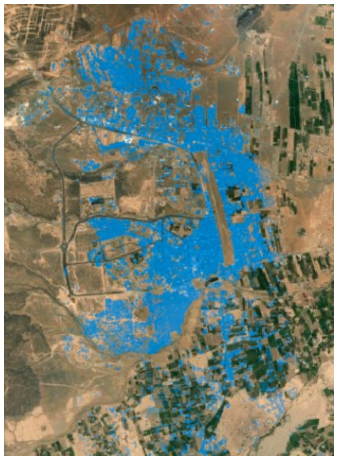

Composite Urban Area Map, apr. 12 km sq – Marib Yemen

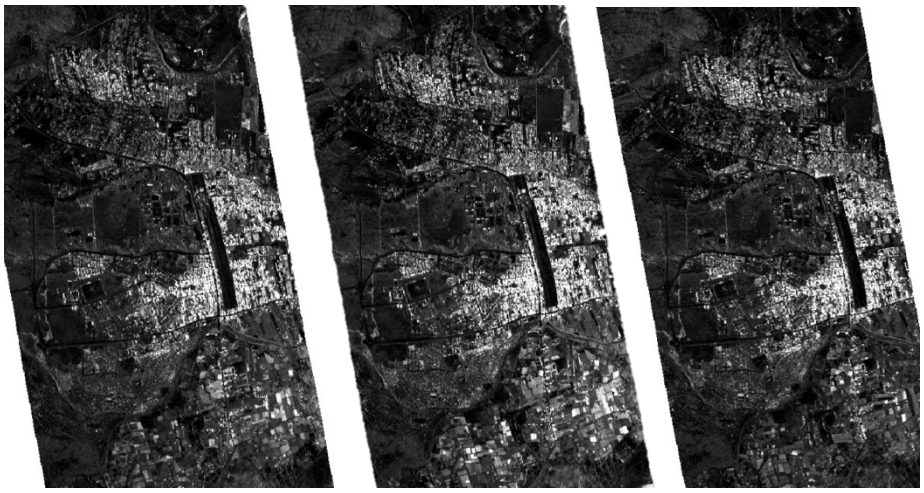

2021-11-18 2021-12-17 2022-03-02

Figure 6 Urban maps derived from a stack of VHR SAR imagery over (left) Marib, Yemen and (right) Gwagwalada, Nigeria plotted on an optical base map. Marib, Yemen – Estimated Urban Area Gwagwalada, Nigeria - Estimated Urban Area.

2. RICE CROP DYNAMICS

As a staple crop for many countries, understand the growth cycle and crop health of rice is critically important in preventing famine and economic instability. Rice cropping presents various backscatter returns in different stages of the phenology due to the double bounce between the growing paddy and water surface [*9*]. This can be used to understand crop dynamics and make yield predictions [*10, 11*]. In several rice-growing regions of the world, the dominant method agricultural production is sustenance farming. Owing to this farm sizes are small, necessitating the use of very high spatial resolution in the remote sensing modality.

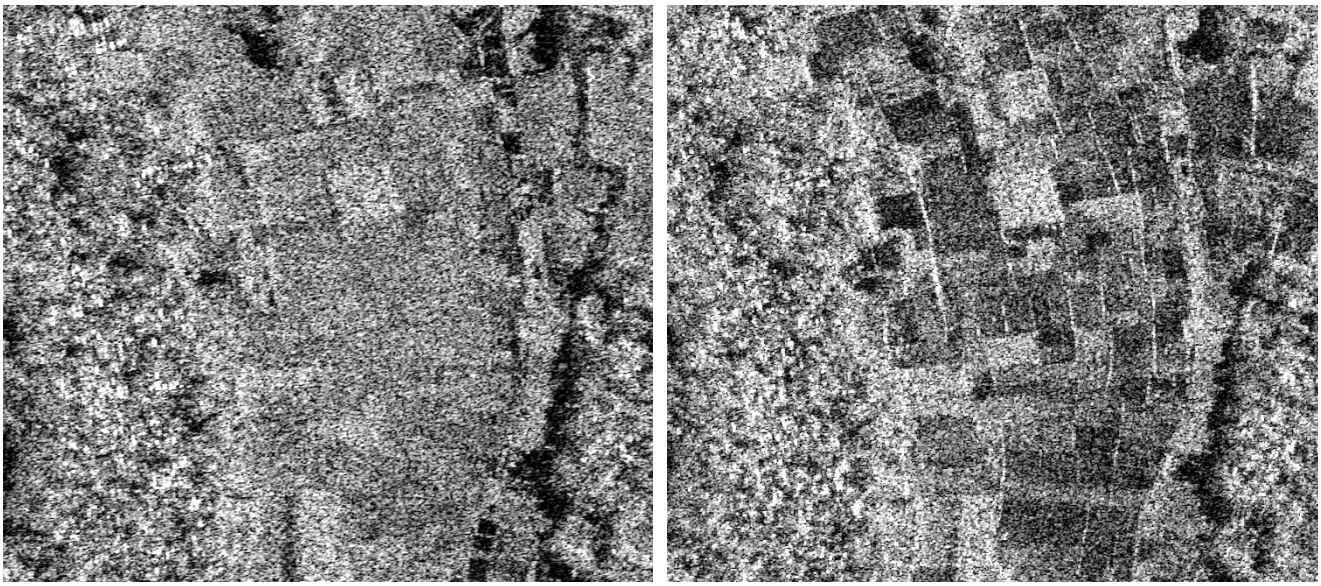

Figure 7 Data collected over Rice growing areas in the growing season (November 2021, left) and in the harvest season (February 2022, right). The backscatter from the rice crop is higher when the crop is mature, compared to the value of the backscatter from the bare soi after harvesting has occurred.

Additionally, depending on access to irrigation, technology, and financial support, different farmers may adopt different harvest and growing cycles. For example, they may use a single cropping pattern that usually has a harvest in the December and January timeframe. Or they may employ a double or triple pattern that have a later harvest. By detecting and classifying the proportion of crops that belong to different cropping patterns, the yield estimates can be updated to be more accurate. While typically all imaging parameters would be matched in the temporal stack to be able to compare backscatter values without adjustment, it might not always be possible, given the limitations of a dynamic constellation primary built to afford customers flexibility in imaging parameters. In the study presented in this paper, the incidence angles vary by appr. 10 degrees among the three collect as follows: acquisition on 2021-11-20 with look angle 35.05, acquisition on 2021-12-01 with look angle 29.63, and acquisition on 2022-02-11 with look angle 38.93. This demonstrates the ability to produce useful outcomes while maintaining imaging flexibility and frequent revisit of the constellation.

There are several ways to normalize for incidence angles. A common way is to perform radiometric terrain correction on the scenes if an appropriate DEM of the area is available. Since for VHR data, this is not always possible, a data driven correction strategy could be used. An area with a constant backscatter throughout the observation period, like a patch of forest is selected in the scene, could be used to normalize the backscatter values of the other AOIs. However as observed in Figure 8, even without a normalization step the point at which harvesting of rice crop occurs is very easy to distinguish. In addition, the different ground cover types consisting of rice paddy that is harvested, rice paddy that continues to grow, forest and water have distinct relative backscatter returns.

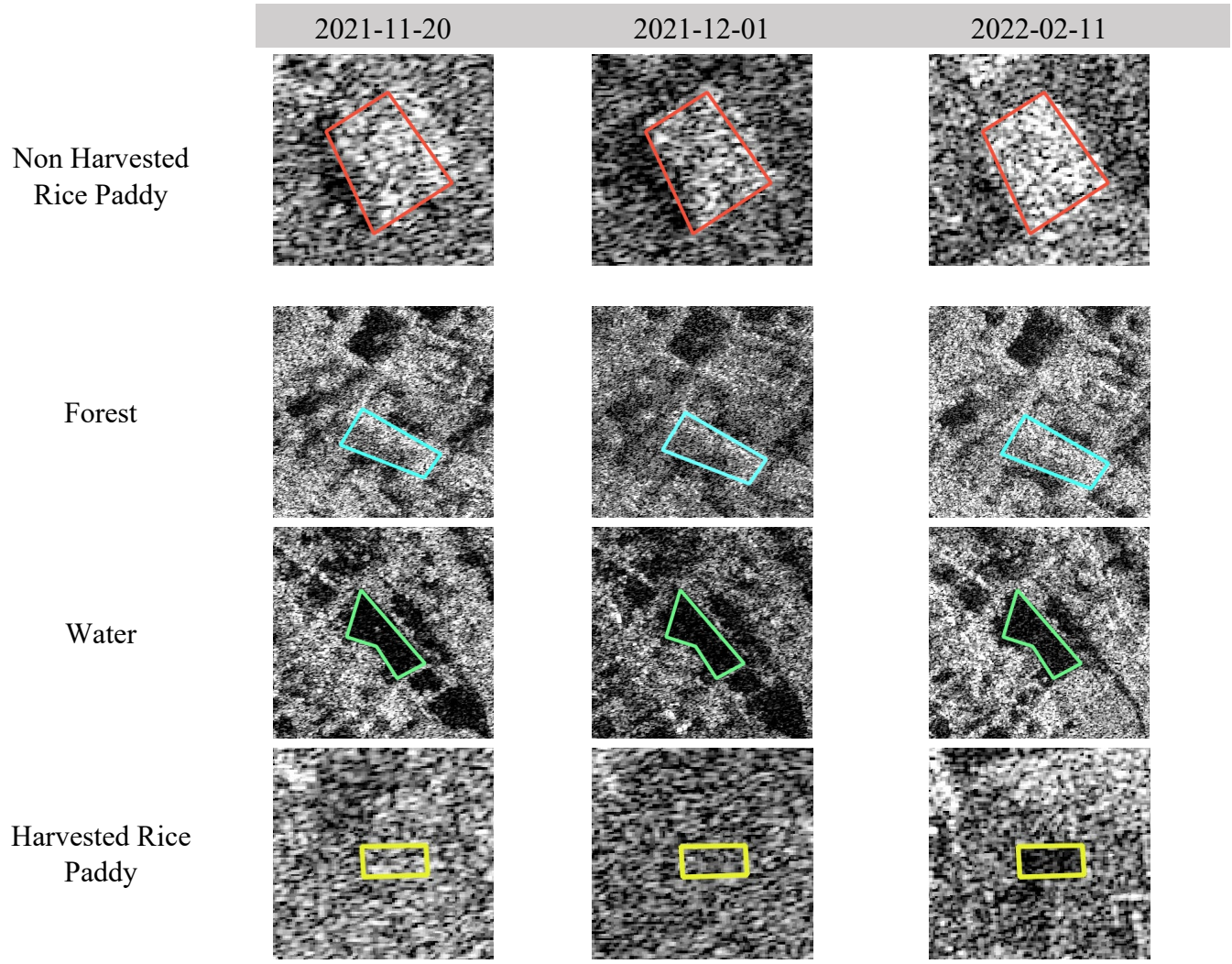

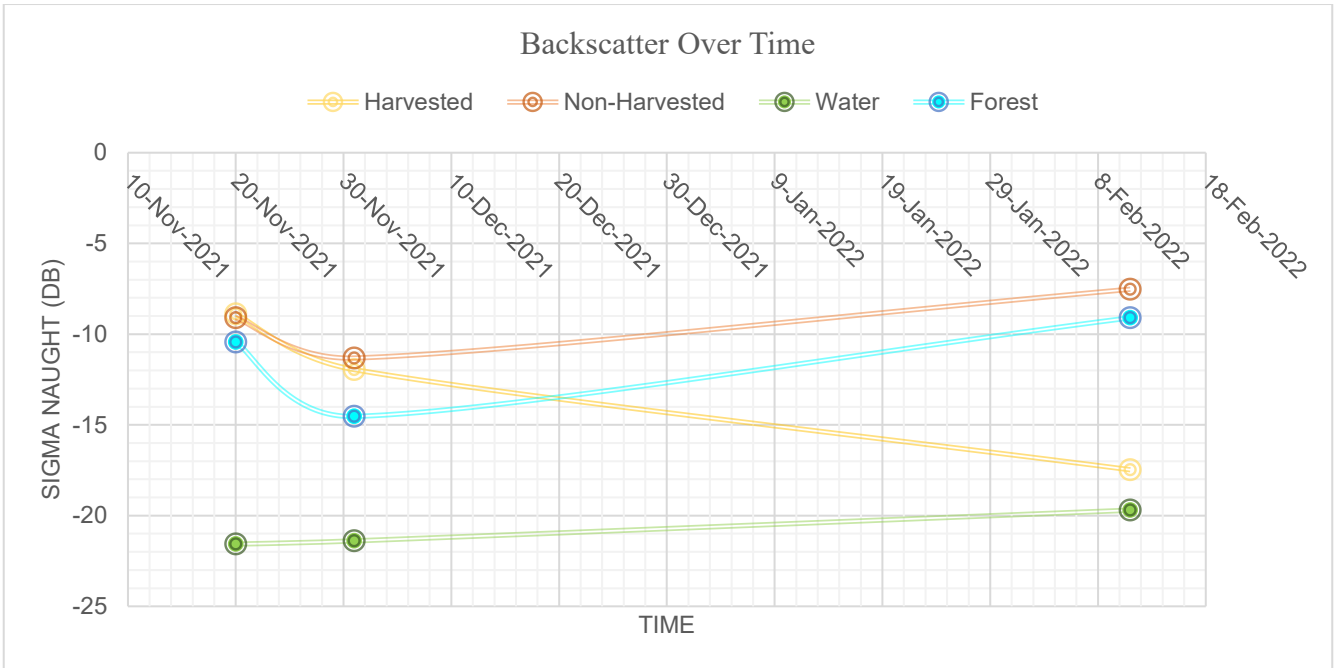

Figure 8 Shows sigma naught backscatter returns in dB from different rice paddy ground cover types. The harvested rice crop sees a sharp drop in backscatter returns in the harvesting cycle, while the unharvested paddy maintains consistent backscatter. This change in backscatter could be exploited for automated classification of agricultural state. Even with a diverse range of collection parameters, the point at which harvesting occurs is easy to discriminate.

3. GLACIERS

Cloud penetration, 24/7 imaging, and large area cover of remote locations make SAR a cost effective and powerful tool for understanding glaciers. SAR data can derive flow velocity, surface elevation change, feed into mass balance models, monitor the calving front location, delineate glacial zones (facies) and other critical parameters [*12, 13*]. Previously, understandings of glacier dynamics have been limited to longer temporal phenomenon, but now a high revisit rate can be exploited to better characterize these movements. Additionally, VHR SAR presents a unique opportunity to better investigate surface flow patterns, superficial ice textures, crevasses, and other surface layer features.

In the case of Cryosphere applications, very high-resolution data which is reflected primarily from the top snow-pack layer (like the case for X-band SAR) provides a unique utility in understanding surface features and tracking them over time. Capella's constellation is ideally suited for this type of mapping. If a robust backscatter model were developed, the accumulation and ablation facies of the glacier could be discriminated at X-band and feed into mass-balance calculations and other metrics that can be useful for tracking glacial health over time. Glacial studies are often performed using airborne systems or in-field measurements, which are costly and limited to planned time periods of the campaign. Remote sensing from space allows for increased flexibility in acquisition times, length of the observation period and periods in which the observations are done.

For this paper, Capella has collected SAR data over two regions and will focus on observations using backscatter returns. The two areas of observation are Ruth Glacier in Denali National Park in the state of Alaska US and the tidewater Helheim Glacier on the southeastern side of Greenland. The collected imagery involves a mix of spotlight and stripmap imaging modes

Note on figures: Images with red squares indicate a 400 pixel by 400 pixel subset that was used to calculate the mean backscatter return. In the two image figures, the left image indicates location of subset (highlighted with red box) while the right image is a zoomed in look at the subset itself. Mean value calculations were performed on raw pixel values and converted to decibel scale for display.

3.1 Glacier Mosaic Observations

As observed in Figure 9, high resolution X-band SAR captures surface features of the Helheim Glacier in extreme detail. Crevasses, fractures, flow directions and other importance surface level features are apparent. The calving front of the Helheim glacier is easily distinguished, along with another facture line forming approximately 0.8 km upstream. Large ice blocks can clearly be distinguished in the ice mélange after the calving front. Tributary flows into the main glacier body can be seen to the North and South. Figure 10 provides an example of an X-band SAR mosaic of Ruth Glacier and detailed imager of various parts along the glacier, including the mouth of the glacier and very long morraines.

Glaciers are composed of many distinct zones but largely separated into two functional areas, the accumulation zone and the ablation zone. The accumulation zone encompasses areas where snow and ice gathers over time, building the mass of the glacier in that section. The ablation zone is a region in which overall snow and ice content are diminishing over time due to melt. The distinct point at which net buildup changes to net loss is called the equilibrium line. This is a very important metric in a glacier as it informs other metrics such as mass balance. The equilibrium line will vary through the year as seasonal rates of freezing and melting vary with local temperatures [*14*].

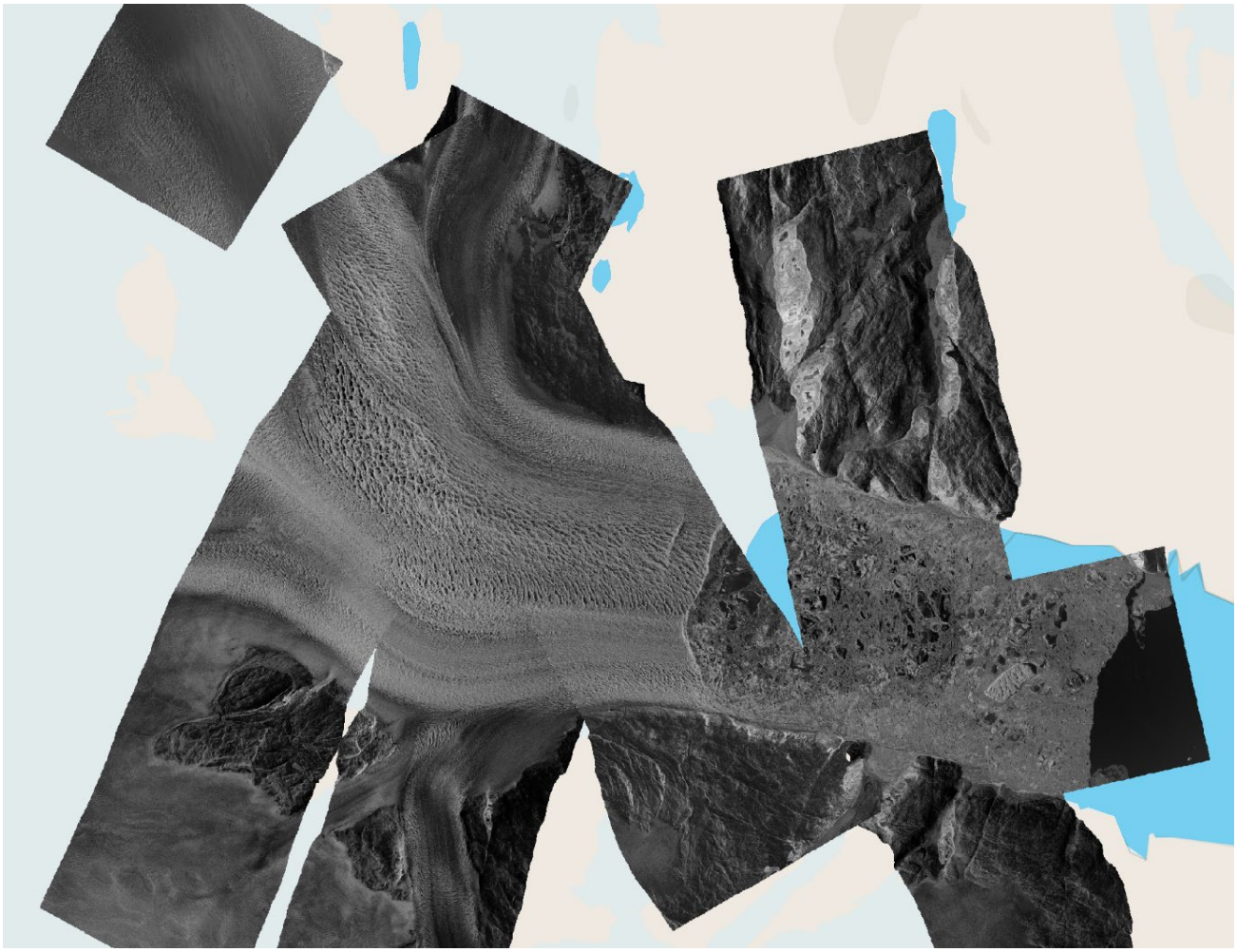

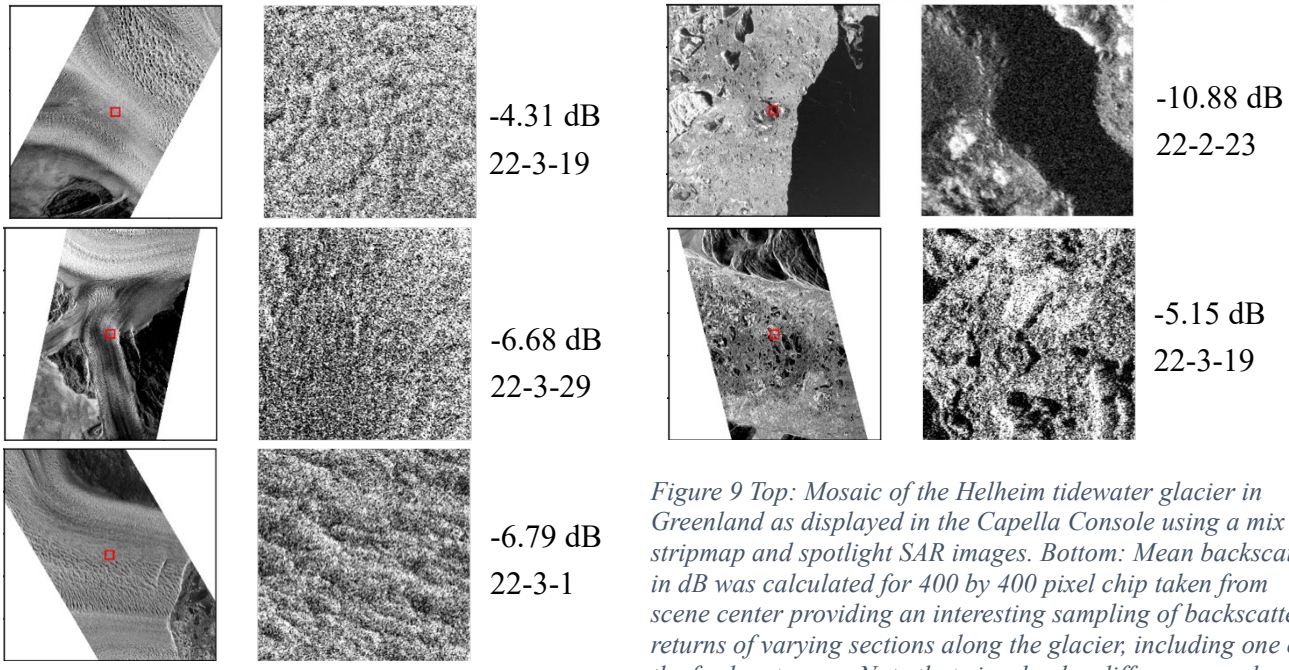

Figure 9 Top: Mosaic of the Helheim tidewater glacier in Greenland as displayed in the Capella Console using a mix of stripmap and spotlight SAR images. Bottom: Mean backscatter in dB was calculated for 400 by 400 pixel chip taken from scene center providing an interesting sampling of backscatter returns of varying sections along the glacier, including one of the feeder streams. Note that visual color difference are largely a function of scaling are not always good indication of absolute return values.

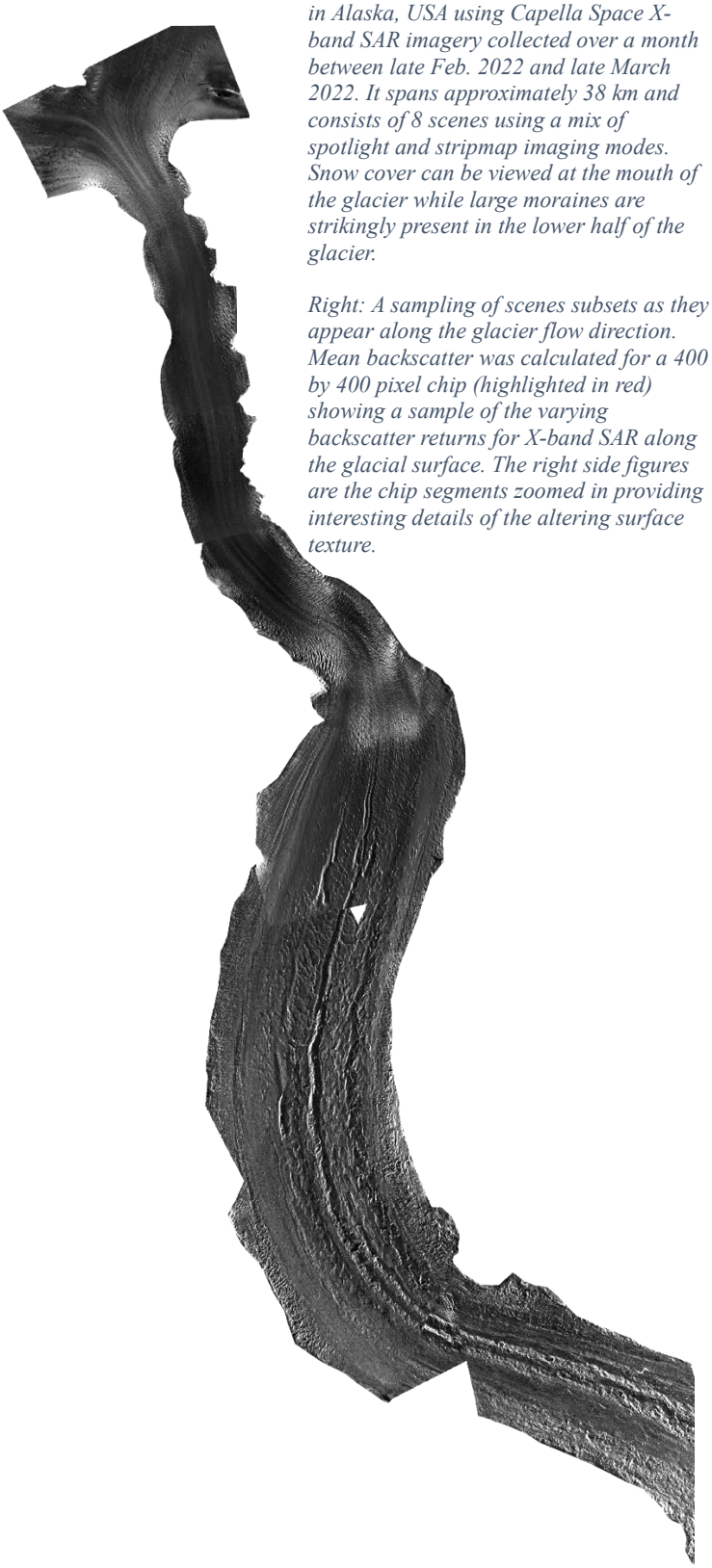

Figure 10 Left: A mosaic of Ruth Glacier in Alaska, USA using Capella Space X-band SAR imagery collected over a month between late Feb. 2022 and late March 2022. It spans approximately 38 km and consists of 8 scenes using a mix of spotlight and stripmap imaging modes. Snow cover can be viewed at the mouth of the glacier while large moraines are strikingly present in the lower half of the glacier.

Right: A sampling of scenes subsets as they appear along the glacier flow direction. Mean backscatter was calculated for a 400 by 400 pixel chip (highlighted in red) showing a sample of the varying backscatter returns for X-band SAR along the glacial surface. The right side figures are the chip segments zoomed in providing interesting details of the altering surface texture.

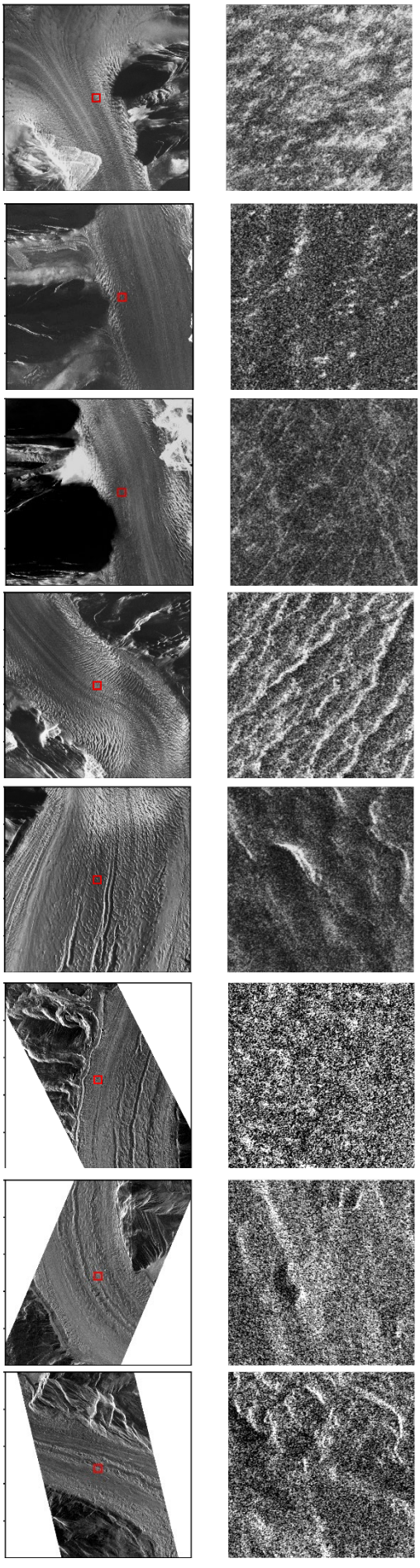

In figure 11, it is possible that the equilibrium line of Ruth Glacier was captured, which is roughly noted with the dashed red line. Without ground truth data it is hard to say for certain. Some promising indications include the very distinct change in backscatter return and the drastic change in surface textures at this point.

This line could be indicating a change from the frozen percolation radar zone to the bare ice radar zone given the time of acquisition at the end of the winter season, when no zones with wet snow or melt would be apparent [10]. The start of large moraines can also be viewed after this point and the natural widening of the glacier body.

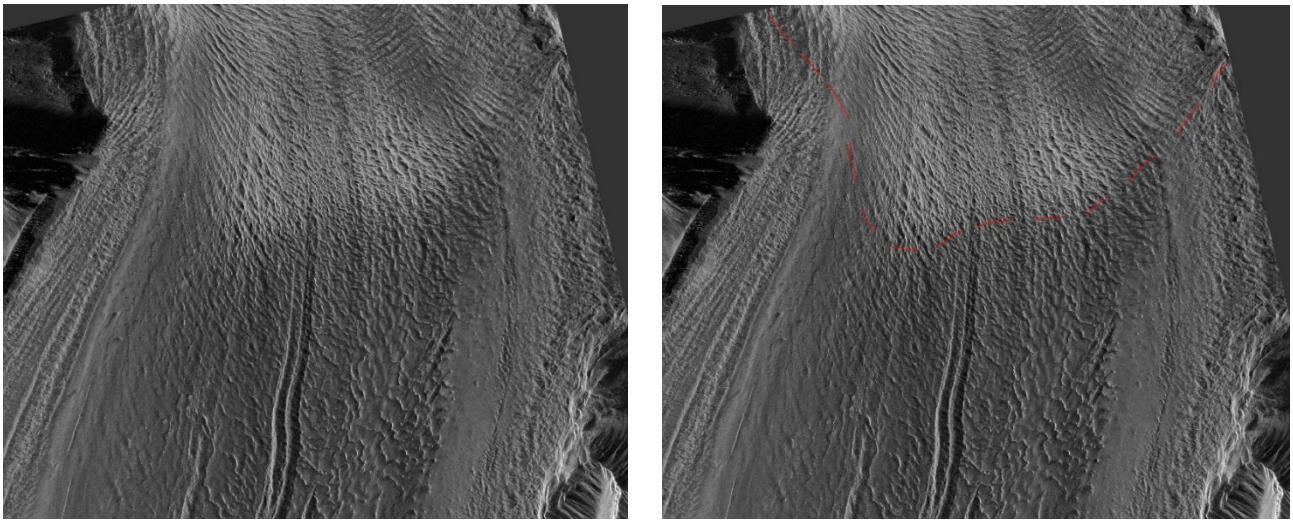

Figure 11 A Capella spotlight image captured over Ruth Glacier on 3/2/22, HH polarization. This region is approximately at the midpoint of the main glacier body and exhibits a clear delineation in backscatter from an area of higher to lower return as it moves downstream. Surface features also change from slightly laterally directed to predominantly downstream where large moraines begin forming.

3.2 Glacier Time Series Observations

Repeated collects, or time series data, are very useful over glaciers because it provides an indication of how they are changing over time. This is useful on multi-annual and interannual time scales.

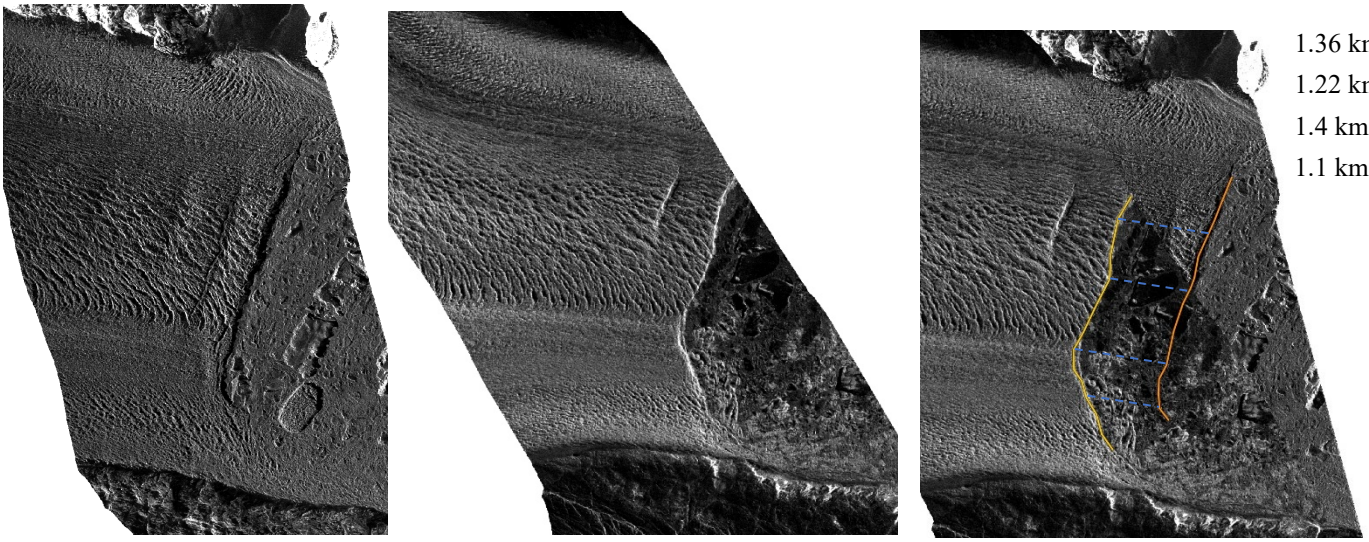

Figure 12 Left is the calving front of the Helheim Glacier from 5/29/21, stripmap image, HH polarization. Middle is the calving front of the Helheim Glacier from 3/1/22, stripmap image, HH polarization. Right is a simple analysis of the calving front movement across the two acquisitions. The calving front receded approximately 1.3 km over the 9-month window

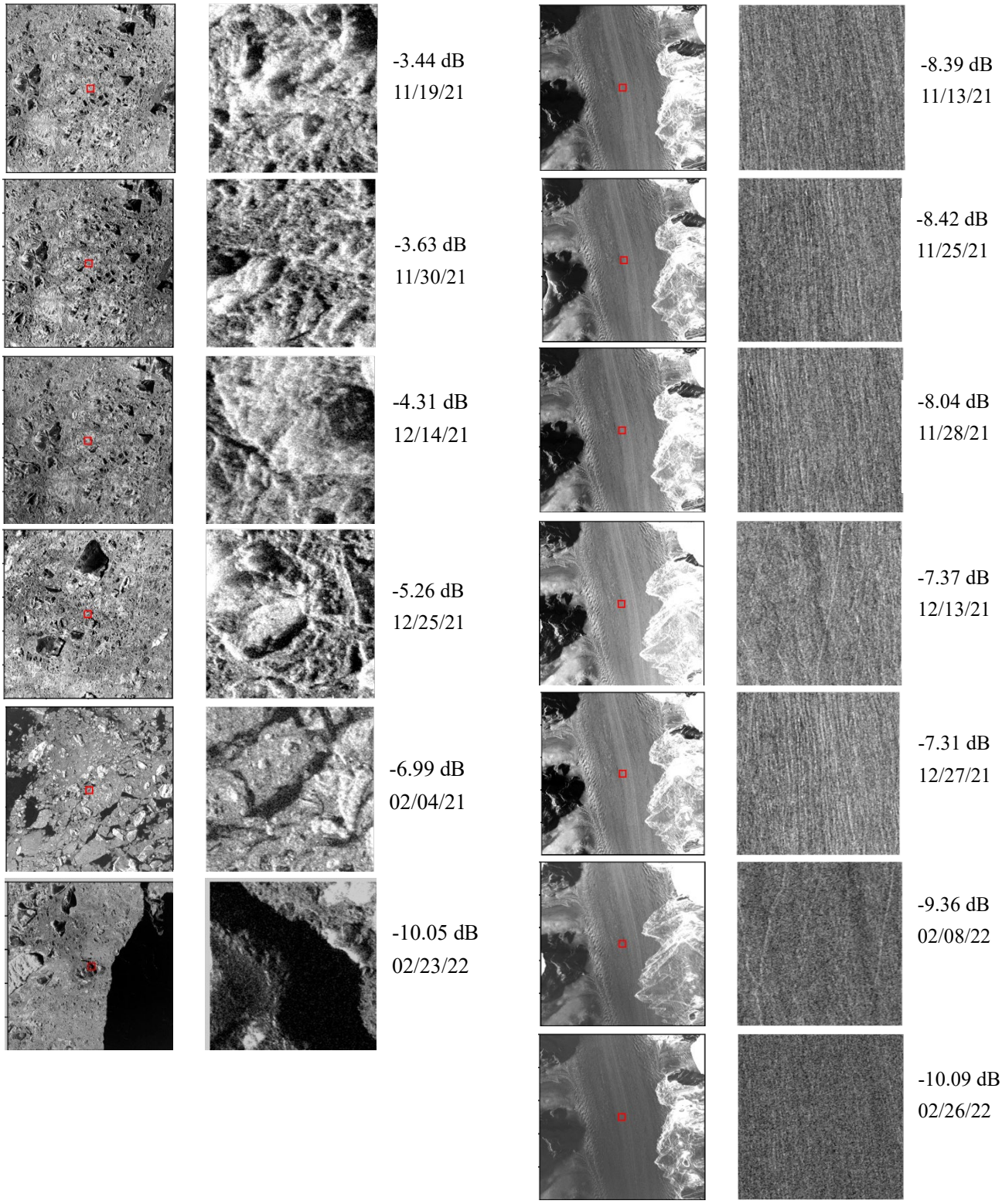

Figure 13 (Left): Repeated Capella Space SAR spotlight acquisitions over an area of the Helheim Glacier past the terminus point as ice mélange progress out to the Sermilik Fjord and ultimately into the Atlantic Ocean. The mean backscatter of the center chip consistently decreased over the observation period from Nov. 2021 to Feb. 2022. Bare sea water can be observed in the last two acquisitions from Feb. 2022, which strongly reduces the mean backscatter. (Right): Repeated Capella Spotlight SAR acquisitions of Ruth Glacier in Denali Nat. Park at approximately 8 km into the glacier body. Backscatter returns are largely consistent over the observation period of about 3 months spanning mid Nov. 2021 to late Feb. 2022. The surface texture interestingly exhibits very fine linear features in the direction of flow. Two contributory flows located just South of Mt. Dickey can be seen in the left images.

A prime example of the utility of time series data is shown in Figure 12, in which the calving front of Helheim Glacier was found to have receded by appr. 1.3 km over a 9 month period between summer 2021 and early spring 2022. Another example application of persistent monitoring is shown in Figure 13 in which surface features and average backscatter for a specific area of Helheim and Ruth Glacier were observed over the winter season. With consistent monitoring, a backscatter model of various areas within the glacier could be determined and tracked over time.

4. DATA PREPERATION

The SAR data was converted into Sigma Naught value in dB using the following equation:

$$\sigma^0_{dB} = 20\log_{10}(Scale\ Factor * DN_{GEO/GEC})$$

The scale factor is a calibration factor reported for each collection in the metadata. DN stands for digital number and is the raw pixel value reported in the image file. GEO and GEC refer to two types of detected SAR data products by Capella Space, Geocoded Terrain Corrected and Geocoded Ellipsoid Corrected respectively. The data used in this presentation is a combination of GEO and GEC file formats.

5. OPEN DATA PROGRAM

All data used for observation and analysis in this paper will be made available to the public. Capella Space has an Open Data Program in which a selection of scenes are made available online via the Capella Space console and through the companion API. Read more about the open data and instructions for accessing here https://www.capellaspace.com/community/capella-open-data/.

6. CONCLUSION

Capella Space is a valuable new source of very high-resolution, high-quality X-band SAR data that can be applied to various applications in earth observation and remote sensing. We have shown just a sample of critical applications in this paper. For the area of infrastructure mapping, SAR data was used to calculate approximate urban ground cover area in Gwagwalada Nigeria and Marib Yemen. Rice crop dynamics were observed in Bangladesh by identifying harvested verse non-harvested rice paddies at different points in the growing season. Observations of Ruth and Helheim Glacier led to the mapping of calving front retreat, backscatter characteristics and surface layer features. We have demonstrated a fraction of the utility that persistent, all-weather, day-and-night SAR can provide, especially in the selected applications due to heavy, seasonal cloud cover and the polar night. This powerful tool can be used to help address some of humanities most pressing challenges. We welcome the community to further expand and develop these techniques to transform information made in space into understandings about our planet.

7. REFERENCES

[1] G. Farquharson, D. Castelletti, C. Stringham and D. Eddy, "An Update on the Capella Space Radar Constellation," EUSAR 2021; 13th European Conference on Synthetic Aperture Radar, 2021, pp. 1-4.

[2] D. Castelletti, G. Farquharson, C. Stringham, M. Duersch and D. Eddy, "Capella Space First Operational SAR Satellite," 2021 IEEE International Geoscience and Remote Sensing Symposium IGARSS, 2021, pp. 1483-1486, doi: 10.1109/IGARSS47720.2021.9554100.

[3] Revision of the World Urbanization Prospects Report, Population Division of the United Nations Department of Economic and Social Affairs (UN DESA), 2018.

[4] Anghel, Andrei, et al. "Combining spaceborne SAR images with 3D point clouds for infrastructure monitoring applications." ISPRS journal of photogrammetry and remote sensing 111 (2016): 45-61.

[5] Abdulkadir Ozden, Ardeshir Faghri, Mingxin Li, and Kaz Tabrizi, “Evaluation of synthetic aperture radar satellite remote sensing for pavement and infrastructure monitoring,” Procedia Engineering, vol. 145, pp. 752–759, 2016.

[6] Jackson, Trisha L., et al. "Parameterization of urban characteristics for global climate modeling." Annals of the Association of American Geographers 100.4 (2010): 848-865.

[7] URL: https://www.visualcapitalist.com/ranked-the-worlds-fastest-growing-cities/, Fetched on 2022-04-08

[8] Jackson, Trisha L., et al. "Parameterization of urban characteristics for global climate modeling." Annals of the Association of American Geographers 100.4 (2010): 848-865.

[9] Xiaodong Huang, Benjamin RK Runkle, Mark Isbell, Beatriz Moreno-Garcia, Heather McNairn, Michele L Reba, and Nathan Torbick, “Rice inundation assessment using polarimetric uavsar data,” Earth and Space Science, vol. 8, no. 3, pp. e2020EA001554, 2021.

[10] Seonyoung Park, Jungho Im, Seohui Park, Cheolhee Yoo, Hyangsun Han, and Jinyoung Rhee, “Classification and map-ping of paddy rice by combining landsat and sar time series data,” Remote Sensing, vol. 10, no. 3, pp. 447, 2018.

[11] F Ribbes, “Rice field mapping and monitoring with radarsat data,” International Journal of Remote Sensing, vol. 20, no. 4, pp. 745–765, 1999.

[12] Eric Rignot, Richard Forster, and Bryan Isacks, “Interferometric radar observations of glaciar san rafael, Chile”, Journal of Glaciology, vol. 42, no. 141, pp. 279-291, 1996.

[13] Pedro Skvarca, Martin Stuefer, and Helmut Rott, “Temporal changes of glaciar mayo and laguna escondida, southern patagonia, detected by remote sensing data”, Global and Planetary Change, vol. 22, no. 1-4, pp. 245-253, 1999.

[14] Rau, Frank, et al. "Radar glacier zones and their boundaries as indicators of glacier mass balance and climatic variability." Proceedings of the 2nd EARSeL Workshop-Special Interest Group Land Ice and Snow. 2000